

# Does the regulation of local excitation-inhibition balance aid in recovery of functional connectivity? A computational account

Anirudh Vattikonda<sup>1</sup>, S. Bapi Raju<sup>1,2</sup>, Arpan Banerjee<sup>3</sup>, Gustavo Deco<sup>4,5</sup>, Dipanjan Roy<sup>1</sup>

<sup>1</sup>Cognitive Science Lab, International Institute of Information Technology, Hyderabad, India

<sup>2</sup>Center for Neural and Cognitive Sciences, University of Hyderabad, India

<sup>3</sup>Cognitive Brain Lab, National Brain Research Centre, NH8, Manesar, India

<sup>4</sup>Center for Brain and Cognition, Computational Neuroscience Group,

Department of Information and Communication Technologies, Universitat Pompeu Fabra, Roc

Boronat 138, Barcelona, 08018, Spain

<sup>5</sup>Institució Catalana de Recerca i Estudis Avançats (ICREA), Universitat Pompeu Fabra,

Passeig Lluís

**Keywords: Resting state networks, Default mode, Virtual lesion, DMF model, Exc-Inh balance, functional connectivity**

## Abstract

Computational modeling of the spontaneous dynamics over the whole brain provides critical insight into the spatiotemporal organization of brain dynamics at multiple resolutions and their alteration to changes in brain structure (e.g. in diseased states, aging, across individuals). Recent experimental evidence further suggests that the adverse effect of lesions are visible on spontaneous dynamics characterized by changes in resting state functional connectivity and its graph theoretical properties (e.g. modularity). These changes originate from altered neural dynamics in individual brain areas that are otherwise poised towards a homeostatic equilibrium

to maintain a stable excitatory and inhibitory activity. In this work, we employ a homeostatic inhibitory mechanism, balancing excitation and inhibition in the local brain areas of the entire cortex under neurological impairments like lesions to understand global functional recovery (across brain networks and individuals). Previous computational and empirical studies have demonstrated that the resting state functional connectivity varies primarily due to the location and specific topological characteristics of the lesion. We show that local homeostatic balance provides a functional recovery by re-establishing excitation-inhibition balance in all areas that are affected by lesion. We systematically compare the extent of recovery in the primary hub areas (e.g. default mode network (DMN), medial temporal lobe, medial prefrontal cortex) as well as other sensory areas like primary motor area, supplementary motor area, fronto-parietal and temporo-parietal networks. Our findings suggest that stability and richness similar to the normal brain dynamics at rest is achievable by re-establishment of balance.

## **1. Introduction**

Whole brain resting state dynamics at macroscopic scale provides a powerful approach to understanding key determinants of normal versus abnormal brain functions. Abnormal resting state brain dynamics characterized by changes in resting state functional connectivity (rs-FC) are observed in neurological disorders like epilepsy (Centeno and Carmichael, 2014; Holmes et al., 2013), Alzheimer's disease (Damoiseaux, 2012), Stroke (Park et al., 2011, Gratton et al., 2012), Schizophrenia (Yang et al., 2014) etc. Several theoretical models have been developed to understand the underlying mechanisms that allow such rich spontaneous dynamics to emerge (Deco et al., 2009, 2014, Hellyer et al., 2016). Local excitation and inhibition (E-I) balance or homeostasis is shown to play a key role in maintaining such rich dynamics. In this study we

investigate how local E-I balance is affected by structural perturbations and whether the same mechanism can aid in functional recovery to normal rs-FC after a focal lesion is introduced in the underlying structure. Previous work in this direction has sought out for computational tools and graph theoretical techniques to investigate the precise impact on rs-FC under virtual lesions in specific brain areas (both interhemispheric and intrahemispheric) (Alstott et al. (2009); Cabral et al. (2012); Arsiwala et al. (2015)). Alstott et al. (2009) and subsequently, Cabral et al. (2012) have independently investigated using computational models the nature of impact on rs-FC due to perturbation in the structural connectivity (SC) similar to what is observed in brain lesions. Further, Cabral et al. (2012) theoretical results suggest that most disconnection-related neuropathology should induce the same qualitative changes in resting-state brain activity and hence, finding common functional network alteration in the resting dynamics under a variety of clinical conditions. These studies are the first ones to highlight the importance of lesion foci; for example, hubs have a potentially damaging impact on the rs-FC to the point of a minimal chance of recovery after lesion (Alstott et al., 2009; Arsiwalla et al., 2015). However, none of the above studies account for fundamental processes like local homeostatic regulation of inhibition providing right E-I balance to adapt to a target excitatory firing rate as a mechanism for functional recovery. For the first time, we demonstrate systematically how this inhibitory homeostasis aid in recovery across lesion foci (whether hub or not) using a variety of cortical parcellations. Recently, Vogels et al., (2011) and Hellyer et al. (2016) have demonstrated in a computational setup that inhibitory synaptic plasticity (a type of homeostatic plasticity) may appropriately balance the excitatory and inhibitory currents of a cortical neuron, thereby rendering it to produce a stable cortical output rather than runaway excitation. In Deco et al. (2014), a feedback inhibition control (FIC) algorithm was proposed to adjust the strength of inhibitory weights recursively and adapt to a target excitatory firing rate of 3 – 4 Hz. In this

study, we investigate how such local E-I balance is disturbed across multiple brain areas including hubs. What is the exact relationship between structural graph properties and the disturbed E-I balance? How widespread is the disturbed E-I balance depending on the lesion foci? We find that restoring the local E-I balance by using recursive adaptation of inhibitory weights in individual brain areas brings the local excitability to a stable firing range without compromising the richness of resting state dynamics and, as a result, reduces the damaging impact on rs-FC over the whole brain. Moreover, resting state networks are implicated in core process of human cognition like integration of cognitive and emotional processing (Greicius et al., 2003), monitoring the world around us (Gusnard et al., 2001) and mind-wandering (Mason et al., 2007). Hence we hypothesize that restoring rs-FC close to normality should aid in recovery from lesion.

## **2 Materials and Methods**

### **2.1 Empirical Structural Connectivity**

The empirical SC matrix used in this paper is generated by using an automated pipeline (Schirner et al., 2015) for reconstruction of fiber tracks from T1 structural MR images and diffusion-weighted images (DWI) acquired from 49 healthy subjects (30 females, 19 males) at Berlin Center for Advanced Imaging, Charité University Medicine, Berlin, Germany. The subjects' age ranged from 18 to 80 years with a mean age of  $41.55 \pm 18.44$ . The images obtained from these scans are used as input to the reconstruction pipeline to generate the SC matrix for each subject (Please refer to Schirner et al. (2015) for a detailed outline of the pipeline for generating SC matrix). In this pipeline, high resolution T1 anatomical images are used to create segmentation and parcellation of cortical and subcortical gray matter, white

matter segments and diffusion weighted imaging (DWI) for generating tractography masks. The major pre-processing steps on T1 anatomical images are skull stripping, removal of non-brain tissue, brain mask generation, cortical reconstruction, motion correction, intensity normalization, WM and subcortical segmentation, cortical tessellation generating GM–WM and GM-pia interface surface-triangulations and probabilistic atlas-based cortical and subcortical parcellation. These parcellations, segmentations and masks are then used to guide the probabilistic tractography algorithm to estimate connection strengths (a value in the range 0 to 1) between each pair of areas in the cortical gray matter parcellation. The parcellation used in this study is Desikan-Killiany parcellation (Desikan et al., 2006) which consists of 68 cortical regions of interest (ROI). SC matrices generated from each subject’s MRI data are averaged element-wise to obtain an averaged SC matrix. The connectivity strength between each pair of 68 areas represents how one area can influence other areas in the context of a specific model (refer to section 2.4). To make sure results reported are robust to resolution of the parcellation and size of lesioned nodes, a SC matrix of 998 ROIs of approximately uniform size (Hagmann et al., 2008) generated from diffusion spectrum imaging of 5 healthy subjects is also used.

## **2.2 Empirical Resting State Functional Connectivity**

Empirical rs-FC matrix is also generated using the same pipeline from the fMRI scans of the 49 subjects used for generating SC. The major steps involved in generating rs-FC matrix are brain extraction, motion correction, six-degrees of freedom (DOF) linear registration to the MNI space and high pass temporal filtering. The BOLD volumes are registered with subject’s T1 weighted anatomical images and parcellated according to Desikan-Killiany atlas (Desikan et al., 2006). BOLD signals from each of the 68 ROIs are computed by taking the mean of BOLD signals of all voxels in that area. Aggregated BOLD time-series of each region is z-transformed and pairwise Pearson correlation coefficient is computed to obtain the rs-FC matrix of each

subject. The FC matrix used in this study is the average of rs-FC matrices of all 49 subjects. Also since we only use resting state functional data in this study, we use the words functional connectivity (FC) and resting state functional connectivity (rs-FC) synonymously.

### **2.3 Simulating virtual focal Lesions**

Focal lesions damage the anatomical structural connectivity of the brain in a specific area or in and around a specific area. In order to simulate a focal lesion in area  $i$  (lesion center), all the connections to and from that area are set to zero in the SC matrix, i.e., all the entries in row  $i$  and column  $i$  of SC matrix are set to zero. An example of virtually lesioned SC matrix with left Precuneus as the lesion center is shown in **Fig. 1**. To understand the characteristics of lesion location that critically impact rs-FC, 68 virtually lesioned SC matrices are generated with focal virtual lesions at each one of the 68 ROIs. For the SC matrix of 998 ROIs a focal lesion in area  $i$  is simulated by disconnecting (set to zero) all connections to and from 50 nearest neighbours (5% of total) in addition to connections of lesion center. Lesions centered at 40 different locations (20 in each hemisphere) covering 80 – 90 % of the cerebral cortex are simulated resulting in 40 lesioned SC matrices at a resolution of 998 ROIs. These matrices are then downsampled to 66 areas by averaging across ROIs (For details on downsampling refer to Hagmann et al., 2008 , Honey et al., 2008).

### **2.4 Computational Model simulating whole brain resting state dynamics**

Mean field models (Wilson and Cowan, 1972, Wong and Wang, 2006, Deco et al., 2009, Hellyer et al, 2016) allow simulation of whole brain dynamics and are analytically tractable unlike models for networks of spiking neurons. Using mean field models earlier research have shown that rs-FC can be estimated from the SC matrix using a large scale cortical dynamic mean field (DMF) model (Deco et al., 2014) and a hemodynamic model (Friston et al., 2000; Friston et al., 2003). The DMF model is a set of coupled stochastic differential equations which

govern the evolution of synaptic gating variables with time (Deco et al., 2014). The hemodynamic model is a set of coupled differential equations which can predict the BOLD responses of a neural population given the synaptic activity of that population. Using the generated BOLD responses from each area, FC can be estimated by computing Pearson correlation coefficient between BOLD responses of each pair of areas. The pipeline used to compute FC using anatomical SC matrix and computational modeling is shown in **Fig. 2**.

*Dynamic Mean Field Model:* In DMF model, each brain area is modeled as a population of excitatory and inhibitory neurons with excitatory NMDA synapses and inhibitory GABA synapses. The computational model for simulating the synaptic activity is given by the set of coupled stochastic nonlinear differential equations given below (Deco et al., 2014).

$$I_i^{(E)} = W_E I_0 + w_+ J_{NMDA} + G J_{NMDA} \sum_j C_{ij} S_j^{(E)} - J_i S_i^{(I)} \quad (1)$$

$$I_i^{(I)} = W_I I_0 + J_{NMDA} S_i^{(E)} - S_i^{(I)} \quad (2)$$

$$r_i^{(E)} = \frac{a_E I_i^{(E)} - b_E}{1 - e^{(-d_E (a_E I_i^{(E)} - b_E))}} \quad (3)$$

$$r_i^{(I)} = \frac{a_I I_i^{(I)} - b_I}{1 - e^{(-d_I (a_I I_i^{(I)} - b_I))}} \quad (4)$$

$$\frac{dS_i^{(E)}}{dt}(t) = -\frac{S_i^{(E)}}{\tau_E} + (1 - S_i^{(E)})\gamma r_i^{(E)} + \sigma v_i(t) \quad (5)$$

$$\frac{dS_i^{(I)}}{dt}(t) = -\frac{S_i^{(I)}}{\tau_I} + r_i^{(I)} + \sigma v_i(t) \quad (6)$$

Here  $I_i^{(E \text{ or } I)}$ , is the input current to area  $i$  and superscripts  $E$  and  $I$  represent excitatory and inhibitory populations in that area.  $r_i^{E \text{ or } I}$  is the population firing rate of excitatory or inhibitory populations of area  $i$ ,  $S_i^{E \text{ or } I}$  is the average synaptic gating variable of area  $i$ .  $I_0$  is the effective external input scaled by  $W_E$  and  $W_I$  for excitatory and inhibitory populations.  $J_{NMDA}$  is the

162 excitatory synaptic coupling and  $J_i$  is the local feedback inhibitory synaptic coupling.  $v_i$  in Eq.  
 163 5,6 is uncorrelated standard Gaussian noise with noise amplitude  $\sigma = 0.001$  nA. The input  
 164 currents to an excitatory population in an area are: recurrent excitatory currents, recurrent  
 165 inhibitory currents, long range excitatory currents from excitatory populations in all other areas,  
 166 and external currents. Long range excitatory currents from other areas to an excitatory  
 167 population in area  $i$  are constrained by the connectivity strength from those areas given by  $C_{ij}$ ,  
 168 where  $C_{ij}$  is the  $ij^{th}$  entry in the SC matrix. Since recurrent excitatory currents are already taken  
 169 into account while computing the input current to an excitatory population all the diagonal  
 170 elements,  $C_{ii}$ , are set to zero in the SC matrix. The connectivity strengths  $C_{ij}$  are scaled by a  
 171 global coupling parameter  $G$ . A parameter sweep for various values of  $G$  is performed to  
 172 compute the optimal value of  $G$  for which the simulated FC-estimate best correlates with that  
 173 computed from the empirical resting-state fMRI data of healthy controls. The input currents to  
 174 an inhibitory population in area  $i$  are: recurrent excitatory currents, recurrent inhibitory currents,  
 175 external currents. All the parameters of the model are set to same values as in Deco et al. (2014)  
 176 and summarized in **Table 2**. Furthermore, in order to maintain a steady state firing rate of 2 – 5  
 177 Hz, the input current to excitatory population is maintained such that  $I_i^E - b_E/a_E = -0.026$  nA (see  
 178 Eq. 3) by the Feedback Inhibition Control (FIC) algorithm, as proposed in Deco et al. (2014).  
 179 The FIC algorithm iteratively adjusts  $J_i$  values representing synaptic coupling from inhibitory  
 180 neurons to excitatory neurons, to maintain the input current at an excitatory population equal to  
 181  $b_E/a_E - 0.026$  nA, with a tolerance of  $\pm 0.005$  nA. Hence we consider local excitation-inhibition  
 182 balance to be established in an area when the input current to an excitatory pool is in the above  
 183 range. By numerically solving the differential equations in this model using Euler's method  
 184 with a step size of 0.1 ms for 8 minutes we generated the synaptic activity of each area and used



this activity as input to the hemodynamic model (Friston et al., 2000, Friston et al., 2003) to generate the resting-state BOLD responses of each brain area. Although we used a time step of 0.1 milliseconds in Euler's method, we sampled the synaptic activity from each area every 1 millisecond. First 500 ms of BOLD responses are truncated to allow for initial transients and the rest is downsampled every 2 s to get a resolution similar to empirical BOLD time series. All simulations are performed using MATLAB.

#### *DMF model parameter space identification and calibration*

Global coupling strength  $G$  is a free parameter of DMF model that scales long range excitatory input. In order to estimate the optimal value of  $G$  that best predicts resting dynamics, DMF model is simulated with increasing values of  $G$  starting from 0 and at increments of 0.025. The model generated FC is compared against empirical FC by calculating the fit between them as Pearson correlation coefficient between the z-transformed upper diagonal elements. The correlation fit between simulated FC and empirical FC as a function of the free parameter  $G$  is shown in **Fig. 3A**. The optimal value of  $G$  is that which gives best correlation fit between empirical and simulated FC while maintaining the firing rate in the range of 3 - 5 Hz in all brain regions. For the SC of 68 areas best correlation fit of 0.6 between simulated and empirical FC while maintaining a low firing rate is observed when  $G = 0.6$ . The firing rate of all regions at this optimal value of  $G$  is shown in **Fig. 3B**. As can be seen in this figure, a low firing rate of about 4 Hz is maintained in all areas in the balanced excitation-inhibition condition. Empirical FC and model-generated FC obtained by simulating DMF model with  $G$  set to 0.6 are shown in **Fig. 3C and D** respectively.  $G$  is set to 0.6 in all the simulations performed in further analysis throughout the entire paper unless otherwise specified. For values of  $G > 0.6$  firing rate of many areas exceed 20 Hz and hence the model is not bio-physically realistic.

## 2.5 Measures for characterizing lesioned nodes and for effects of lesion on FC

To characterize areas into hubs or connector nodes, graph theoretical measures, namely, *participation coefficient* and *node strength* are used. Brain Connectivity Toolbox (Rubinov and Sporns, 2010) is used to compute both these measures. Frobenius norm of the difference between model predicted FC matrix and empirical FC matrix is used to measure the dynamic effects of a lesion on FC

*Participation Coefficient:* Given the modular organization of a graph *participation coefficient* of each node in that graph can be computed (Guimera and Amaral, 2005). Participation coefficient measures how well distributed the links of a node are to other modules. If the links of a node are uniformly distributed to all modules then its participation coefficient is 1, whereas if all its links are within its own module then participation coefficient is 0. So nodes with participation coefficient close to 1 are considered as connector nodes. Eq. 7 describes how to compute the participation coefficient of  $i^{th}$  node, where  $N_M$  is the number of modules,  $k_{is}$  is the number of links of node  $i$  to module  $s$  and  $k_i$  is the total number of links of node  $i$ .

$$P_i = 1 - \sum_{s=1}^{N_M} \left( \frac{k_{is}}{k_i} \right) \quad (7)$$

*Node Strength* is the sum of connection strengths of all connections to that area. Nodes with high node strength are shown to have relatively large effect on FC when lesioned compared with nodes with low node strength (Alstott et al., 2009). Eq. 8 describes how to compute node strength of  $i^{th}$  area, where  $N$  is the number of ROIs.

$$Strength(area_i) = \sum_{j=1}^N C_{ij} \quad (8)$$

Note that for higher resolution SC, participation coefficient and node strength are computed as summation of participation coefficient and node strength respectively of all 50 disconnected ROIs for each lesion.

*FC Distance (FCD)*: In order to measure the similarity or distance between the model predicted FC and the empirical FC, we have used the Frobenius norm of the difference between the two FC matrices.

$$FCD = \sqrt{\sum_{i=1}^N \sum_{j=1}^N |FCEmpirical(i, j) - FCModel(i, j)|^2} \quad (9)$$

Higher the FC Distance, higher the damaging impact of lesion on FC. Similarly, lower the FC Distance, lower is the impact. Eq. 9 describes how FC distance between these two matrices is computed.

*Z-score*: We used Z-scores to test the hypothesis that whether the functional correlations of any pair of ROI before and after lesion are from different distributions. Before computing the Z-scores we have converted both FC matrices, predicted by DMF model using healthy controls SC and lesioned SC, to normal distribution by using Fisher's z-transform. Z-score between functional correlation of area  $i$  and  $j$  is computed as

$$Z_{ij} = \frac{(r_{ij}^{healthy} - r_{ij}^{lesioned})}{\sqrt{\left(\frac{1}{df-3} + \frac{1}{df-3}\right)}} \quad (10)$$

Where,  $df$  is the effective degrees of freedom and it is equal to 230 (length of simulated BOLD time series) for all the simulations in this study. To find a threshold for Z-score above which correlations are considered to have come from different distributions, we have computed Z-

scores between correlations of two FC matrices generated by averaging FC from two sets of 5 independent runs of model using healthy controls SC. For  $|Z| > 2$  the error rate is zero, hence Z-scores ( $|Z|$ ) greater than 2 are considered to have significantly changed.

## **2.6 Measuring immediate effects of lesion on FC**

We define *immediate effects* as those effects on FC that are caused by a lesion, before processes like plasticity set in to recover the damage caused by lesion. We are not directly modeling plasticity but rather the E-I balance that maintains local homeostasis. In fact, E-I balance has been shown to be related to inhibitory synaptic plasticity (Vogels et al., 2011). Hence, we consider the effects due to a lesion in SC matrix on the FC before re-establishing E-I balance as immediate effects. We start with an E-I balanced network of healthy subjects and study the effect of acute brain injury or lesion on these networks. In order to measure the immediate effects on FC arising from a lesion in one of the 68 ROIs, we have used the following procedure (refer to the model described by Eq. 1-6): 1) We have computed the  $J_i$  values, i.e., local feedback inhibitory synaptic coupling, of each brain area by running the DMF model with FIC algorithm using the averaged SC of healthy controls. These are the values that maintain E-I balance before lesion. 2) Using these  $J_i$  values and a virtually lesioned SC in DMF model we generated the FC as described above in the model section. 3) Finally, we compute FC Distance between empirical FC and model generated FC to quantify the effects of a particular lesion on FC. Note that step 1 is a one-time process, as the SC of healthy controls does not change, however steps 2 and 3 must be run for each lesioned SC.

## **2.7 Re-establishing Excitation-Inhibition balance after a lesion**

In this study we show that the impact of cortical lesions on functional connectivity can be reduced by re-establishing E-I balance. Recall that E-I balance would be perturbed by such lesions. After virtually lesioning an ROI we observe that many other ROIs lose E-I balance

causing immediate effect on FC. We hypothesize that if E-I balance is re-established after lesion then the impact of lesion on FC would be reduced. In order to investigate this we use the following procedure: 1) We have initialized the  $J_i$  values i.e., local feedback synaptic coupling weights with the values obtained by running DMF model with FIC on the averaged SC of healthy controls. 2) Using the lesioned SC we run the DMF model with FIC to re-establish E-I balance in all the areas. 3) To measure the similarity between model-generated FC and empirical FC, we compute the FC distance between these two matrices. Again step 1 is a one-time process whereas steps 2 and 3 are repeated for each virtually lesioned SC matrix.

### 3 RESULTS

#### 3.1 Effects of lesion on E-I balance

An area, say  $i$ , is considered to have E-I balance if  $I_i^E - \frac{b_E}{a_E} = -0.026$  nA with a tolerance of  $\pm 0.005$  nA (see Materials and Methods), where  $I_i^E$  is excitatory input current to area  $i$ ,  $b_E$  and  $a_E$  are intrinsic parameters used in estimating average firing rate of an excitatory population (Deco et al., 2014). Hence we consider an area to have lost E-I balance if  $|I_i^E - \frac{b_E}{a_E} + 0.026| > 0.005$ , where  $|x|$  is the absolute value of  $x$ . **Fig. 4A** shows that local E-I balance is perturbed in many areas when SC, obtained with left Precuneus (IPCUN) as the lesion center, is used in the DMF model. **Fig. 4B** shows the number of areas that have lost E-I balance for each of the 68 brain areas as lesion centers in the virtually lesioned SC matrix. We then investigated the relationship between lesioned area's participation coefficient and the effect on E-I balance. **Fig. 4C** exhibits, lesions in areas with high participation coefficient perturb

balance in a wider number of areas. Participation Coefficient and number of areas that have lost E-I balance have shown a strong correlation of 0.61 ( $p < 0.001$ ) (see **Fig. 4C**). To make sure that the results observed are not due to non-uniform lesion sizes, correlation between participation coefficient and number of areas that lost E-I balance is investigated on a SC of higher resolution with 40 lesions of uniform size (see Materials and Methods). Similar results are observed (**Fig. S1 A**) with a correlation of 0.56 ( $p < 0.001$ )

### **3.2 Immediate effects of lesion on functional connectivity**

Next we investigated the immediate effects on FC for each lesion center. In order to predict the immediate effects on FC we have initialized the inhibitory synaptic weights ( $J_i$ ) with the values corresponding to E-I balanced condition. Then a specific focal lesion is incorporated in the SC matrix and the resulting FC is generated using the DMF model (see Materials & Methods). We then computed the FC distance between the model-predicted FC and empirical FC. The FC distance is found to be strongly correlated to the participation coefficient and node strength of the lesion center. Node strength and FC Distance showed a correlation of 0.87 ( $p < 0.001$ ) and participation coefficient and FC Distance showed a correlation of 0.62 ( $p < 0.001$ ) (see **Fig. 6A and B (black)**). Same relationship is observed even when the lesions are of uniform size (**Fig. S1 B**). This finding is consistent with previous studies (Alstott et al., 2009) i.e., if the lesioned area is a hub or connector node (that has high participation coefficient or node strength) then the effects due to a lesion on FC are generally large. Although in the main text we highlight the recovery process based on lesion center in IPCUN, several experiments with lesion centers in other areas were conducted and the results are similar (See Supplementary Material and Table 3)

### **3.3 Functional recovery after re-establishing E-I balance**

319 After re-establishing local E-I balance in all areas, by simulating the DMF model with FIC and  
320 initializing  $J_i$  with those generated by simulating DMF model with FIC on SC of healthy  
321 controls (see Materials & Methods), we found that the impact of lesion on FC is significantly  
322 reduced compared to the immediate impact of lesion (shown in previous section) on FC. For  
323 example, FC predicted by the DMF model using a virtually lesioned SC with lesion center as  
324 IPCUN before and after re-establishing E-I balance are shown in **Fig. 5**. The FC predicted by  
325 model after re-establishing E-I balance is similar to the empirical FC than the FC predicted by  
326 the model before re-establishing E-I balance. Unlike in the case of immediate impact of lesion  
327 on FC, we found that by re-establishing E-I balance in all areas FC Distance is not so strongly  
328 correlated with participation coefficient and node strength of lesioned area. This is illustrated by  
329 reduced correlations between node strength, participation coefficient and FC Distance to 0.25 ( $p$   
330 = 0.04) and 0.03 ( $p = 0.82$ ), respectively as shown in **Fig. 6A, B (blue)**. The results are again  
331 validated using a SC with lesions of uniform size (**Fig. S1 B**). Previous studies (Alstott et al.,  
332 2009) have shown that lesion impact is higher when the lesioned area is near cortical midline.  
333 We found that even when areas near the cortical midline (PCUN, CAC) are lesioned, by re-  
334 establishing E-I balance the effects of lesion on FC have been largely reduced. Table 3 gives a  
335 summary of effects of lesions in cortical midline, parietal and temporal cortex, frontal cortex,  
336 sensory, motor cortex. **Fig. 7 (top)** shows the functional connections that have significantly  
337 changed ( $|z| > 2$ ) immediately after a lesion in cortical midline (ICAC). By re-establishing E-I  
338 balance the number of connections that have significantly changed have been largely reduced as  
339 shown in **Fig. 7 (bottom)**. One important observation to be noted is that the impact of lesion on  
340 intra-hemispheric connections is reduced drastically after re-establishing E-I balance. Similar  
341 results are observed for lesions in frontal cortex (CMF) and parietal cortex (IP) as shown in  
342 supplementary material (see **Fig. S2, S3**). It can be clearly seen that the number of connections

that have significantly changed are drastically reduced after re-establishing E-I balance. This shows that compared to the FC predicted by DMF model immediately after lesion, there is a significant FC recovery after E-I balance is re-established.

#### *FC Recovery across subjects:*

FC recovery across subjects is compared by using SC of 5 different subjects. First, optimal value of  $G$  is computed for each subject's SC. Optimal value of  $G$  varied across subjects in the range 0.5 to 0.8. For all 5 subjects, FC recovery results are qualitatively similar to the average SC case i.e. even when hubs are lesioned, after re-establishing E-I balance the effects of lesion on FC are largely reduced. **Fig. 8** shows how FC distance varies across subjects before and after re-establishing E-I balance when regions which are more likely to be hubs (participation coefficient  $> 0.5$ ) are lesioned. Finally, we looked at how local inhibitory weights of each area ( $J_i$  values) changed across lesion location after re-establishment of E-I balance. To investigate this relationship, correlation between updated  $J_i$  value of an area for each lesion and participation coefficient of the lesion center is computed. For all areas, the updated  $J_i$  values showed strong correlation ( $r > 0.35$ ,  $p < 0.001$ ) with participation coefficient of lesioned location. Hence we posit that when hubs are lesioned there is an increased excitatory activity in all areas driving the dynamics towards a high excitatory regime.

## **4 Discussion**

Whole brain computational modeling is becoming increasingly popular for gaining a deeper neurophysiological understanding of complex brain functions. In particular, assessing the effect of short-range (recurrent connectivity) and long-range (inter/intra-hemispheric) input during



resting and task conditions may provide valuable insight into resources allocated to processing noisy as well as structured information (Deco, G. et al., 2014; Deco, G. & Kringelbach, M. L et al., 2014; Roy et al., 2014). The brain regulates such information flow from region to region based on principles of integration as well as segregation (Deco et al., 2015). We argue that whole-brain computational modeling based on underlying anatomical connectivity obtained from neuroimaging data can be used to gain new insights into such segregation and integration processes. The motivation for our present study stems from the need for understanding whether recurrent inhibitory weight up-and-down regulation meaning homeostasis can indeed aid in functional recovery to normalcy under a variety cortical lesions spread over multiple lesion centers. However there are several limitation to this study. Firstly unlike recently implemented by Hellyer et al. (2016) inhibitory plasticity is not directly modeled however all the ingredients are present and the underlying homeostatic mechanisms are qualitatively very similar to qualify this as a good candidate for inhibitory plasticity. While their whole purpose of introducing inhibitory plasticity is to predict accurately empirical FC our's is not. We are carefully looking at the departure from E-I balanced regime due to change in excitation resulted from a lesion. This may vary across subjects and lesion centers. Hence, we make a comparison between how the recurrent inhibitory weights change based on location of lesion foci and across participants. We do find variability in the adaptation time to the appropriate  $J_i$  values based on the size or location of the lesion but not significant variability across participants. For the overall mathematical tractability which was established in our earlier work with this model (Deco et al. (2014); Roy et al. (2014)) DMF model is chosen in the current work. One of the major advantages of using DMF model is that it allows for tracking mathematically long-range excitatory inputs to relevant brain areas either due to variation in the global coupling strength or by the perturbation introduced by the lesioned SC. In a recent study (Yang et al.,

2014), such a large-scale mathematical model has been used to show key model parameters global coupling strength, recurrent self-excitatory weights might be responsible for the empirically observed high power of the total signal in schizophrenia patients. In this work, we regulate the recurrent inhibitory weights in individual brain areas for the maintenance of regional E-I balance under focal lesion. We quantify the lesion impact on E-I balance area wise using the correlation between participation coefficient of lesioned area and the degree of perturbation in the E-I balance. Our investigation is carried out over the entire Cerebral Cortex much like in the spirit of previous lesion modeling attempts made by Alstott et al. (2009); Cabral et al. (2012), Arshiwala et al. (2015), Adhikari et al. (2015). For the first time, our study systematically characterizes departure from healthy E-I balance (**Fig. 4 A,B,C**) due to focal lesions in brain modules (hub areas like DMN, FPN and sensory areas like Visual, Motor, etc. ). Further, it is computationally demonstrated how cortical recovery to normalcy is possible using a simple local inhibitory homeostasis mechanism (similar to inhibitory plasticity as proposed by Helleyer et al. (2016)) with lesion centers covering over 80% of the cerebral cortex (**Table 2**). We have shown that upon lesioning a node which acts as a hub or connector node there is a widespread disruption in the regional E-I balance (see **Table 1**; rPCUN, rPC, rISTH, rCAC, IPCUN, IPC, lISTH, lCAC prefixes r,l stand for right and left hemisphere respectively). Interestingly, these areas are located in the vicinity of Supplementary motor area (SMA), Primary motor cortex (M1) which are directly affected following focal lesions in stroke patients. We have shown that immediate effects of an injury on FC are significant when the lesioned node is a hub using a similarity measure such as FC distance (see Material and Methods). This finding is consistent with the previous computational studies (Alstott et al., 2009; Arsiwalla et al., 2015). We have also shown that upon re-establishing E-I balance in all areas excluding lesioned area the effects of an injury on FC are dramatically reduced even when

414 the lesioned area is a hub. We believe this finding is of importance in designing strategies for  
415 brain network recovery. Virtual lesions generated in this study are focal (composed of default  
416 mode brain areas, frontoparietal, temporoparietal junctions) that are commonly found in  
417 structural aberrations present in the stroke (Awad et al., 1986). Previously lesions of posterior  
418 medial cortex (PMC) were described as rare, but resulting in profound disorders of  
419 consciousness (Damasio et al., (1999)), while lesions of the dorsal anterior cingulate cortex  
420 (dACC) resulted in severe disruptions of personality and even emotional processing, resulting in  
421 apathy and inattention (Bush et al., (2000)). Lesions in the vicinity of temporoparietal junctions  
422 have been found to be affecting language-related disorders, in particular, the left angular gyrus  
423 has been implicated in dyslexia (Horwitz et al. (2002)), while lesions centered on the posterior  
424 position of right superior temporal cortex (rSTC) often result in spatial hemineglect (Karnath et  
425 al., (2001)). Our modeling approach in the present article indeed demonstrates computationally  
426 to recover from the widespread spatial disruption induced by lesioned brain areas. Moreover,  
427 our model suggests that the pattern of endogenous neural activity, in particular, the default  
428 mode network activity (DMN) can be restored to a significant extent (see **Table 2**). DMN has  
429 been implicated as a common brain network involved in the pathophysiology of aging and  
430 neurodegenerative disorders such as schizophrenia, Alzheimers, autism spectrum disorders  
431 (Douaud, G. et al., (2014)). An eventual restoration of the topology of resting-state FC may aid  
432 in cognitive repair and recovery.

433 One more limiting fact of our study is that, although, we have theoretically shown that recovery  
434 is possible by re-establishing E-I balance, the biological time scale of such process is an open  
435 question. Biologically how long would it take (meaning time scale) for recurrent inhibitory  
436 weights to adapt to a value such that input to the excitatory pool equal to  $I_i^E - b_E / a_E = -0.026$

437 nA i.e., slightly inhibitory dominated, leading to a target firing rate equal to 3.0631 Hz is  
438 difficult to answer? We have checked the variability of  $J_i$  values as a function of the lesion  
439 center and subject wise to get an idea of the numerical time scale of adaptation. Finally, it is  
440 also important to consider the differences in the recovery processes across lesion locations as  
441 well as the difference in simulated FC following re-establishment of E-I balance and healthy  
442 control FC. E-I balance plays a key role in maintaining stable neuronal activity and proper  
443 cortical function. Dynamic interaction between excitatory and inhibitory inputs was shown to  
444 maintain neural networks in a balanced state that favors neural computations (McCormick,  
445 2002; Haider and McCormick, 2009). We have shown that stable neuronal activity after a lesion  
446 is attained by re-establishing E-I balance, through appropriate regulation of the strength of local  
447 inhibition in individual brain areas. However, even after re-establishing E-I balance the FC is  
448 not completely similar to healthy controls FC, as evident from **Fig. 7**, **Fig. S2** and **Fig. S3**,  
449 suggesting that there might be some irrecoverable components, which may result in subtle  
450 differences in a given task performance. Also, the degree of FC recovery as measured by FCD  
451 in **Fig. 8A, B** is not exactly uniform across lesion locations implying that different lesions may  
452 still cause different subtle behavioural deficits based on lesion location. Apart from maintaining  
453 E-I balance, inhibition in local cortical circuits is also shown to play a key role in gain  
454 modulation (Mitchell and Silver, 2003), improving the dynamic range of input representation  
455 (Liu et al., 2011) in cortex, tuning of cortical neurons to sensory stimuli (Wilent and Contreras,  
456 2005; Wang et al., 2000) and pacing oscillations that allow propagation of neuronal signals  
457 (Atallah and Scanziani, 2009; Hasenstaub et al., 2005). Hence changes in the strength of local  
458 inhibition, while maintaining E-I balance, may have an effect on information representation and  
459 transmission in cortex and discrimination performance of the incoming stimuli. One way to  
460 quantify the differences after recovery that potentially impacts information transmission

461 efficacy and stimulus discrimination ability is to measure multi-scale entropy, mutual  
462 information or Fisher information. Further, network measures based on graph theory such as  
463 local efficiency, global efficiency may provide valuable insights into how information routing  
464 changes after reestablishing E-I balance. Existing studies using empirical neuroimaging data  
465 from stroke patients have already shown that there is a change in the modular organization of  
466 resting state functional networks post-stroke (Gratton et al., 2012). Hence a systematic  
467 investigation of graph theoretic properties of FC after re-establishing balance might be a fruitful  
468 avenue for a future study. Another intriguing possibility is to look at the fitting of optimal  
469 underlying structural connectivity (SC) based on recovered functional connectivity (FC) using  
470 an optimization algorithm proposed in Deco et al. (2014b). Compared to normal FC re-  
471 established FC may be working at a different working point of the global workspace. In this  
472 study the long-range coupling strength ( $G$ ) is kept fixed at 0.6 for all simulations; however,  
473 post-stroke SC determines how the global coupling value  $G$  is shifted in the parameter space. In  
474 Deco et al. (2014b), a dramatic improvement of the fitting of the matrices was obtained with the  
475 addition of a small number of anatomical links, particularly cross-hemispheric connections, and  
476 reweighting of existing connections. Like previous study, we suggest that the notion of a critical  
477 working point ' $G$ ', where the structure-function interplay is maximal, may provide a new way  
478 to link behaviour and cognition, and a new perspective to understand recovery of function under  
479 variety of clinical conditions.

480 Currently, longitudinal data acquisition from stroke patients is underway, and it may be possible  
481 to find out how long it would take for meaningful biological recovery. As a future application  
482 we would like to integrate our study into the Virtual Brain Neuroinformatics Platform (Leon et  
483 al., 2013; Ritter et al., 2013; Roy et al., 2014) and would be made available to the clinicians.  
484 Recovery from a variety of lesion locations may allow clinicians to introduce virtual surgery

and simulate the resulting brain dynamics before actually taking any relevant decisions. To match the real-time clinical settings the size of the simulation will have to be significantly scaled, and complexity of the model needs to take into account more brain regions, different neurotransmitters, inhibitory subtypes. Here, the replicability of our finding is checked with multiple levels of granularity of the connectivity data (coarser to finest resolution). If methods to directly measure the target excitation value in a population are available, it might be possible to use techniques such as Transcranial Magnetic Stimulation (TMS), Transcranial Direct Current Stimulation (tDCS) to look at the variability of the excitatory population firing rate with the size and location of the inhibited brain hot spots. In conclusion, in this paper we provide a direct functional benefit of inhibitory homeostatic regulation to bring back the functional connectivity to normalcy and provide stability without compromising the richness and complexity of spatiotemporal dynamics in the brain.

## **Acknowledgements**

This study was funded by A.B. Ramalingaswami fellowship (BT/RLF/Re-entry/31/2011) and Innovative Young Bio-technologist Award (IYBA), (BT/07/IYBA/2013) from Department of Biotechnology, Ministry of Science & Technology, Government of India. GD is supported by the ERC Advanced Grant: DYSTRUCTURE (n. 295129), by the Spanish Research Project PSI2013-42091-P. and funding from the European Union Seventh Framework Programme (FP7-ICT Human Brain Project (grant no. 60402)).

## **References**

Adhikari, M. H., Beharelle, A. R., Griffa, A., Hagmann, P., Solodkin, A., McIntosh, A. R., ... & Deco, G. (2015). Computational Modeling of Resting-State Activity Demonstrates Markers of

508 Normalcy in Children with Prenatal or Perinatal Stroke. *The Journal of Neuroscience*, 35(23),  
509 8914-8924.

510

511 Alstott, J., Breakspear, M., Hagmann, P., Cammoun, L., & Sporns, O. (2009). Modeling the  
512 impact of lesions in the human brain. *PLoS Comput Biol*, 5(6), e1000408-e1000408.

513

514 Arsiwalla, X. D., Zucca, R., Betella, A., Martinez, E., Dalmazzo, D., Omedas, P., ... &  
515 Verschure, P. F. (2015). Network dynamics with BrainX3: a large-scale simulation of the  
516 human brain network with real-time interaction. *Frontiers in neuroinformatics*, 9.

517

518 Awad, I., Modic, M., Little, J. R., Furlan, A. J., & Weinstein, M. (1986). Focal parenchymal  
519 lesions in transient ischemic attacks: correlation of computed tomography and magnetic  
520 resonance imaging. *Stroke*, 17(3), 399-403.

521

522 Bush, G., Luu, P., & Posner, M. I. (2000). Cognitive and emotional influences in anterior  
523 cingulate cortex. *Trends in cognitive sciences*, 4(6), 215-222.

524

525 Cabral, J., Hugues, E., Kringelbach, M. L., & Deco, G. (2012). Modeling the outcome of  
526 structural disconnection on resting-state functional connectivity. *Neuroimage*, 62(3), 1342-1353.

527

528 Centeno, M., & Carmichael, D. W. (2014). Network connectivity in epilepsy: resting state fMRI  
529 and EEG-fMRI contributions. *Frontiers in neurology*, 5.

530

531 Damoiseaux, J. S. (2012). Resting-state fMRI as a biomarker for Alzheimer's disease.  
532 *Alzheimers Res Ther*, 4(8).

533

534 Damasio, A., & Dolan, R. J. (1999). The feeling of what happens. *Nature*, 401(6756), 847-847.

535

536 Deco, G., Jirsa, V., McIntosh, A. R., Sporns, O., & Kötter, R. (2009). Key role of coupling,  
537 delay, and noise in resting brain fluctuations. *Proceedings of the National Academy of*  
538 *Sciences*, 106(25), 10302-10307.

539

540 Deco, G., & Jirsa, V. K. (2012). Ongoing cortical activity at rest: criticality, multistability, and  
541 ghost attractors. *The Journal of Neuroscience*, 32(10), 3366-3375.

542

543 Deco, G., Ponce-Alvarez, A., Mantini, D., Romani, G. L., Hagmann, P., & Corbetta, M. (2013).  
544 Resting-state functional connectivity emerges from structurally and dynamically shaped slow  
545 linear fluctuations. *The Journal of Neuroscience*, 33(27), 11239-11252.

546

547 Deco, G., Ponce-Alvarez, A., Hagmann, P., Romani, G. L., Mantini, D., & Corbetta, M. (2014).  
548 How Local Excitation–Inhibition Ratio Impacts the Whole Brain Dynamics. *The Journal of*  
549 *Neuroscience*, 34(23), 7886-7898.

550

551 Deco, G., McIntosh, A. R., Shen, K., Hutchison, R. M., Menon, R. S., Everling, S., ... & Jirsa,  
552 V. K. (2014). Identification of optimal structural connectivity using functional connectivity and  
553 neural modeling. *The Journal of Neuroscience*, 34(23), 7910-7916.

554

555 Deco, G., & Kringelbach, M. L. (2014). Great expectations: using whole-brain computational  
556 connectomics for understanding neuropsychiatric disorders. *Neuron*, 84(5), 892-905.

557



558 Deco, G., Tononi, G., Boly, M., & Kringelbach, M. L. (2015). Rethinking segregation and  
559 integration: contributions of whole-brain modelling. *Nature Reviews Neuroscience*, 16(7), 430-  
560 439.

561

562 Desikan, R. S., Ségonne, F., Fischl, B., Quinn, B. T., Dickerson, B. C., Blacker, D., ... &  
563 Killiany, R. J. (2006). An automated labeling system for subdividing the human cerebral cortex  
564 on MRI scans into gyral based regions of interest. *Neuroimage*, 31(3), 968-980.

565

566 Douaud, G., Groves, A. R., Tamnes, C. K., Westlye, L. T., Duff, E. P., Engvig, A., ... &  
567 Johansen-Berg, H. (2014). A common brain network links development, aging, and  
568 vulnerability to disease. *Proceedings of the National Academy of Sciences*, 111(49), 17648-  
569 17653.

570

571 Friston, K. J., Harrison, L., & Penny, W. (2003). Dynamic causal modelling. *Neuroimage*, 19(4),  
572 1273-1302.

573

574 Friston, K. J., Mechelli, A., Turner, R., & Price, C. J. (2000). Nonlinear responses in fMRI: the  
575 Balloon model, Volterra kernels, and other hemodynamics. *NeuroImage*, 12(4), 466-477.

576

577 Gratton, C., Nomura, E. M., Pérez, F., & D'Esposito, M. (2012). Focal brain lesions to critical  
578 locations cause widespread disruption of the modular organization of the brain. *Journal of*  
579 *cognitive neuroscience*, 24(6), 1275-1285.

580

581 Guimera, R., & Amaral, L. A. N. (2005). Functional cartography of complex metabolic  
582 networks. *Nature*, 433(7028), 895-900.

583

584 Hagmann, P., Cammoun, L., Gigandet, X., Meuli, R., Honey, C. J., Wedeen, V. J., & Sporns, O.  
585 (2008). Mapping the structural core of human cerebral cortex. *PLoS Biol*, 6(7), e159.

586

587 Hellyer, P. J., Jachs, B., Clopath, C., & Leech, R. (2016). Local inhibitory plasticity tunes  
588 macroscopic brain dynamics and allows the emergence of functional brain  
589 networks. *NeuroImage*, 124, 85-95.

590

591 Holmes, M. J., Yang, X., Landman, B. A., Ding, Z., Kang, H., Abou-Khalil, B., ... & Morgan,  
592 V. L. (2013). Functional networks in temporal-lobe epilepsy: a voxel-wise study of resting-state  
593 functional connectivity and gray-matter concentration. *Brain connectivity*, 3(1), 22-30.

594

595 Honey, C. J., Sporns, O., Cammoun, L., Gigandet, X., Thiran, J. P., Meuli, R., & Hagmann, P.  
596 (2009). Predicting human resting-state functional connectivity from structural connectivity.  
597 *Proceedings of the National Academy of Sciences*, 106(6), 2035-2040.

598

599 Horwitz, B., Rumsey, J. M., & Donohue, B. C. (1998). Functional connectivity of the angular  
600 gyrus in normal reading and dyslexia. *Proceedings of the National Academy of*  
601 *Sciences*, 95(15), 8939-8944.

602

603 Karnath, H. O., Ferber, S., & Himmelbach, M. (2001). Spatial awareness is a function of the  
604 temporal not the posterior parietal lobe. *Nature*, 411(6840), 950-953.

605

606 Leon, P. S., Knock, S. A., Woodman, M. M., Domide, L., Mersmann, J., McIntosh, A. R., &  
607 Jirsa, V. (2013). The Virtual Brain: a simulator of primate brain network dynamics. *Frontiers in*  
608 *neuroinformatics*, 7.

609

610 Liu, B. H., Li, Y. T., Ma, W. P., Pan, C. J., Zhang, L. I., & Tao, H. W. (2011). Broad inhibition  
611 sharpens orientation selectivity by expanding input dynamic range in mouse simple cells.  
612 *Neuron*, 71(3), 542-554.

613

614 Mitchell, S. J., & Silver, R. A. (2003). Shunting inhibition modulates neuronal gain during  
615 synaptic excitation. *Neuron*, 38(3), 433-445.

616

617 Park, C. H., Chang, W. H., Ohn, S. H., Kim, S. T., Bang, O. Y., Pascual-Leone, A., & Kim, Y.  
618 H. (2011). Longitudinal changes of resting-state functional connectivity during motor recovery  
619 after stroke. *Stroke*, 42(5), 1357-1362.

620

621 Ritter, P., Schirner, M., McIntosh, A. R., & Jirsa, V. K. (2013). The virtual brain integrates  
622 computational modeling and multimodal neuroimaging. *Brain connectivity*, 3(2), 121-145.

623

624 Roy, D., Sigala, R., Breakspear, M., McIntosh, A. R., Jirsa, V. K., Deco, G., & Ritter, P. (2014).  
625 Using the virtual brain to reveal the role of oscillations and plasticity in shaping brain's  
626 dynamical landscape. *Brain connectivity*, 4(10), 791-811.

627

628 Rubinov, M., & Sporns, O. (2010). Complex network measures of brain connectivity: uses and  
629 interpretations. *Neuroimage*, 52(3), 1059-1069.

630

631 Schirner, M., Rothmeier, S., Jirsa, V. K., McIntosh, A. R., & Ritter, P. (2015). An automated  
632 pipeline for constructing personalized virtual brains from multimodal neuroimaging data.  
633 *NeuroImage*.

634

635 Schoonheim, M. M., Geurts, J. J., Landi, D., Douw, L., van der Meer, M. L., Vrenken, H., ... &  
636 Stam, C. J. (2013). Functional connectivity changes in multiple sclerosis patients: a graph  
637 analytical study of MEG resting state data. *Human brain mapping*, 34(1), 52-61.

638

639 Vogels, T. P., Sprekeler, H., Zenke, F., Clopath, C., & Gerstner, W. (2011). Inhibitory plasticity  
640 balances excitation and inhibition in sensory pathways and memory networks. *Science*,  
641 334(6062), 1569-1573.

642

643 Wang, J., Caspary, D., & Salvi, R. J. (2000). GABA -A antagonist  
644 of tuning in primary auditory cortex. *Neuroreport*, 11(5), 1137-1140.

645

646 Wilent, W. B., & Contreras, D. (2005). Dynamics of excitation and inhibition underlying  
647 stimulus selectivity in rat somatosensory cortex. *Nature neuroscience*, 8(10), 1364-1370.

648

649 Wilson, H. R., & Cowan, J. D. (1972). Excitatory and inhibitory interactions in localized  
650 populations of model neurons. *Biophysical journal*, 12(1), 1.

651

652 Wong, K. F., & Wang, X. J. (2006). A recurrent network mechanism of time integration in  
653 perceptual decisions. *The Journal of neuroscience*, 26(4), 1314-1328.

654

Xia, M., Wang, J., & He, Y. (2013). BrainNet Viewer: a network visualization tool for human brain connectomics. *PloS one*, 8(7), e68910.

Yang, G. J., Murray, J. D., Repovs, G., Cole, M. W., Savic, A., Glasser, M. F., ... & Anticevic, A. (2014). Altered global brain signal in schizophrenia. *Proceedings of the National Academy of Sciences*, 111(20), 7438-7443.

## Figures and Tables Captions:

**Figure 1:** Simulating focal lesions. In order to simulate lesion in an area all the connections to and from that area are set to zero. **A**, Averaged structural connectivity matrix of healthy subjects and the **B**, Lesioned structural connectivity with lesion center as left Precuneus(PCUN) **C**, All the 68 brain areas plotted as spheres according to their Talairach coordinates on the brain surface with all their connections, size of spheres represent the participation coefficient of that area with larger size representing larger participation coefficient. **D**, The connections in **C** that are removed or set to zero when lesioned area is left Precuneus are shown in red.

**Figure 2:** General Pipeline to elucidate estimation of functional connectivity from anatomical structural connectivity. Using the anatomical structural connectivity (SC) obtained from DTI scans, the Dynamic Mean Field (DMF) model generates the synaptic activity for each ROI. These activities are fed as input to Balloon-Windkessel hemodynamic model to generate BOLD time series for each area and finally pairwise Pearson correlation coefficient is calculated to obtain the resting state functional connectivity (FC).

**Figure 3:** Parameter space exploration for optimal value of global coupling strength ( $G$ ) and network dynamics generated by simulating dynamic mean field model with feedback inhibition control using the averaged structural connectivity of 49 healthy subjects: **A**, Correlation fit between simulated functional connectivity and empirical functional connectivity for average SC of healthy controls for various values of global coupling strength.  $G=0.6$  (green cross) produced the best correlation fit of 0.6 while maintaining a low firing rate in all areas. **B**, Firing rate of all regions is maintained below 5 Hz by recursively adjusting the local feedback inhibition weights. **C**, Averaged empirical functional connectivity of 49 healthy subjects. **D**, Model predicted resting state functional connectivity using optimal value of  $G$  and averaged SC of healthy controls.

**Figure 4:** Effects of lesion on E-I balance: Immediately after lesioning, many areas lost their local E-I balance. **A-left**,  $E-I$  balance test condition\* value for each of the 68 brain regions immediately after lesioning left Precuneus. **A-right**,  $E-I$  balance test condition\* values of each area after re-establishing E-I balance. The red line indicates the value below which E-I balance is maintained. **B**, Number of areas that lost local E-I balance with each of the 68 brain regions as lesion center. The number of areas that lost local E-I balance is strongly correlated with the participation coefficient of the lesion center. **C**, Correlation between participation coefficient of each lesion center and the number of areas that lost local E-I balance.

$E-I$  balance test condition\* value for an area  $i$ :  $\left| I_i^E - \frac{b_E}{a_E} + 0.026 \right|$

**Figure 5:** Functional connectivity predicted by DMF model using a virtually lesioned structural connectivity matrix with lesion center as left Precuneus **A**, immediately after lesion i.e without re-establishing E-I balance. **B**, after re-establishing E-I balance

**Figure 6:** Immediate lesion effects and recovery of functional connectivity after cortical lesion. The immediate effects of lesion are strongly correlated with lesion measures: lesioned Node Strength and Participation Coefficient. **A** (black), **B** (black), Correlation between FC Distance and Lesioned Node Strength, FC Distance and Participation Coefficient. FC Distances are computed between model predicted functional connectivity immediately after lesioning each of the 68 brain regions and empirical functional connectivity. **A** (blue), **B** (blue), Correlation between FC Distance and Lesioned Node Strength, FC Distance and Participation Coefficient. FC Distances are computed between model predicted functional connectivity after re-establishing E-I balance in all areas and empirical functional connectivity.

**Figure 7:** Number of connections that significantly changed ( $|Z| > 2$ ), see Materials and Methods, due to lesion in right CAC. The top 3 figures display connections that have significantly changed before re-establishing local E-I balance. The bottom 3 figures represent the connections that have significantly changed after re-establishing local E-I balance. In the lateral view of left and right hemispheres only intra-hemispheric connections are shown while in the dorsal view of the whole brain (middle panel) inter hemispheric connections are also shown. The effects of lesion on both hemispheres have been drastically reduced by re-establishing E-I balance. The number of connections that significantly changed within ipsi-lateral hemisphere is reduced by 97% and within contra-lateral hemisphere by 100%.

**Figure 8:** FC recovery to normalcy across subjects and lesion location. FC Distance across subjects is plotted for lesions at nodes with participation coefficient  $> 0.5$ . **A**, FC Distance across subjects and lesion location immediately after lesion. **B**, FC Distance across subjects and lesion location after re-establishing E-I balance.

**Table 1:** List of all 34 ROIs in each hemisphere. AreaID represents the order of ROIs in the structural and functional connectivity matrices for each hemisphere.

**Table 2:** DMF model parameters and their values used in simulations.

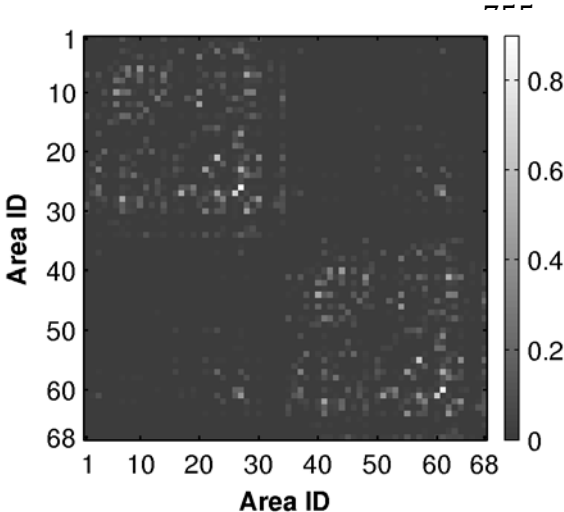
**Table 3:** FC Distance (FCD) before and after re-establishing local E-I balance with lesion centers in cortical midline, parietal and temporal cortex, frontal cortex, sensory and motor cortex. For areas highlighted in bold (IIP, ICMF, rCAC. Here prefixes r, l stand for right and left hemisphere respectively) the functional connections that have significantly changed from healthy controls functional connections are shown in supplementary figures.



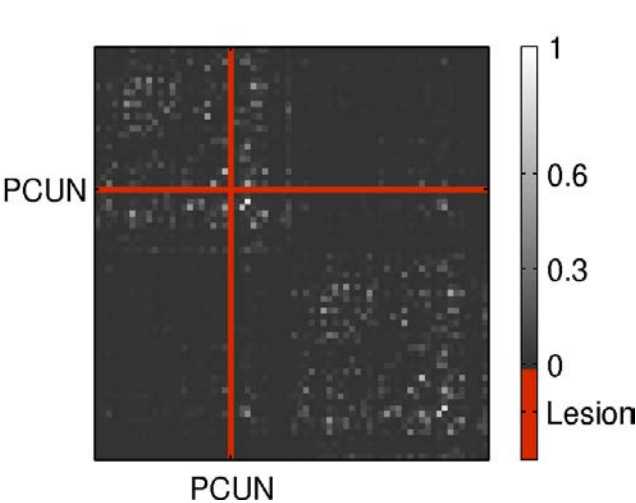
**Figures and Tables:**

**Figure 1:**

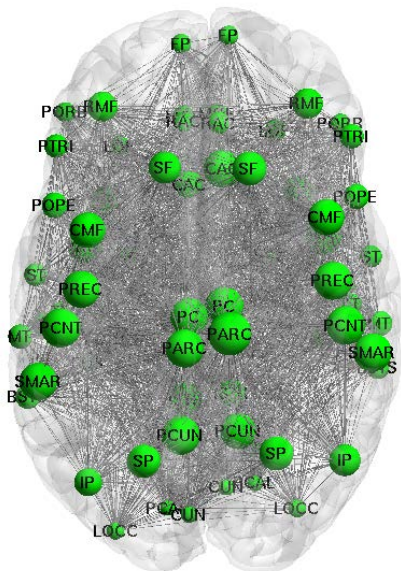
**A**



**B**



**C**



**D**

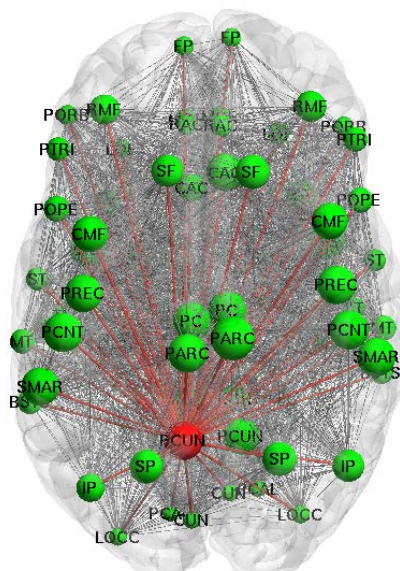


**Figure 2:**

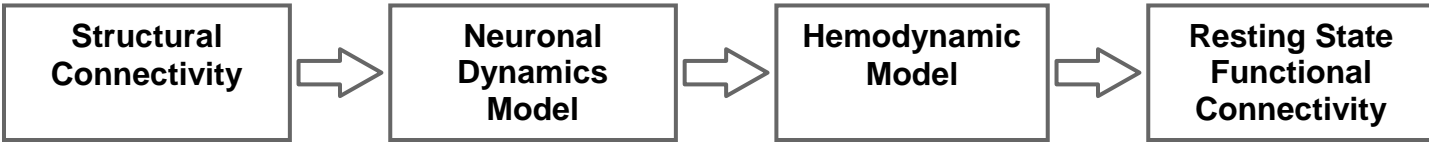


**Figure 3:**

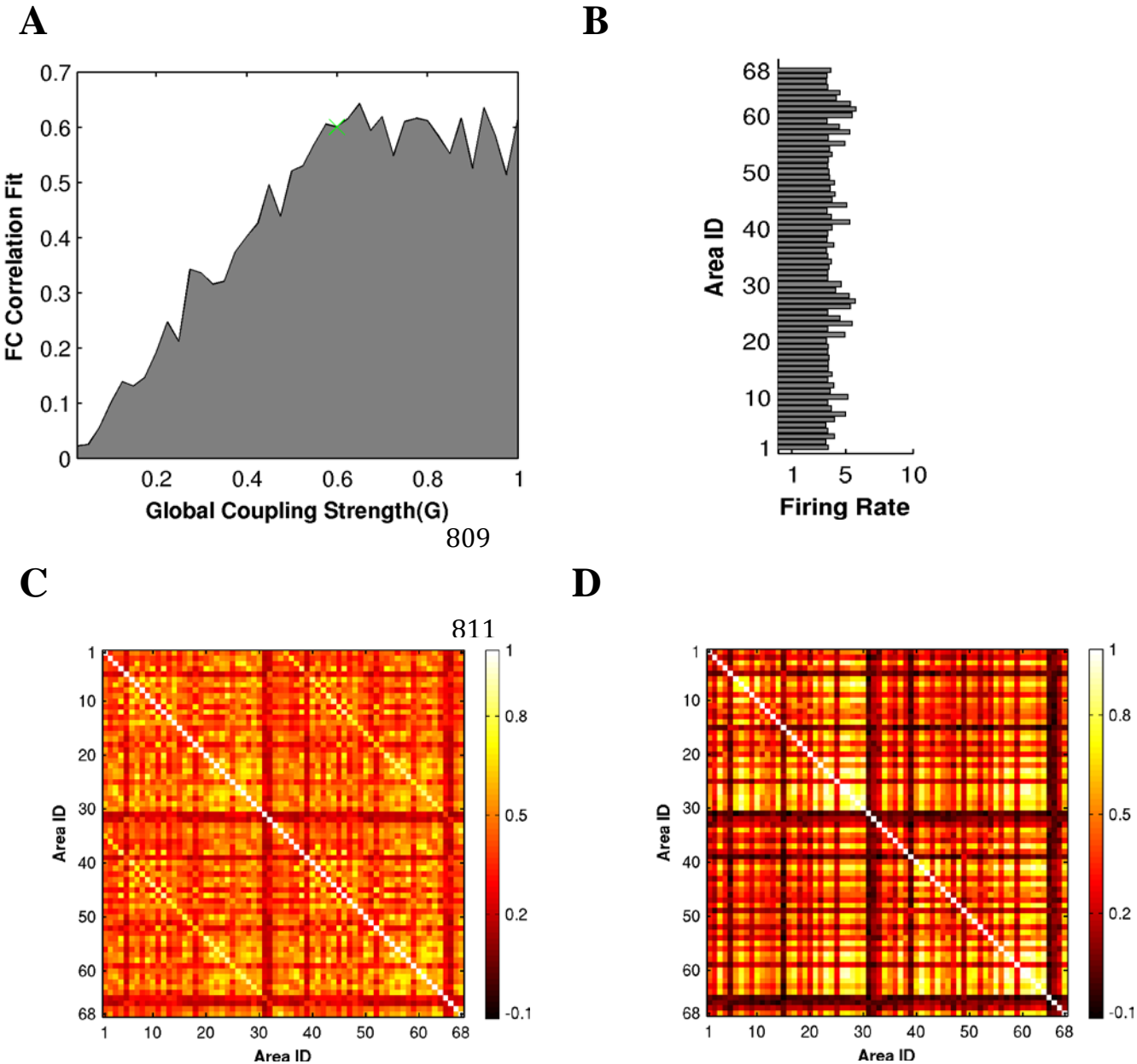
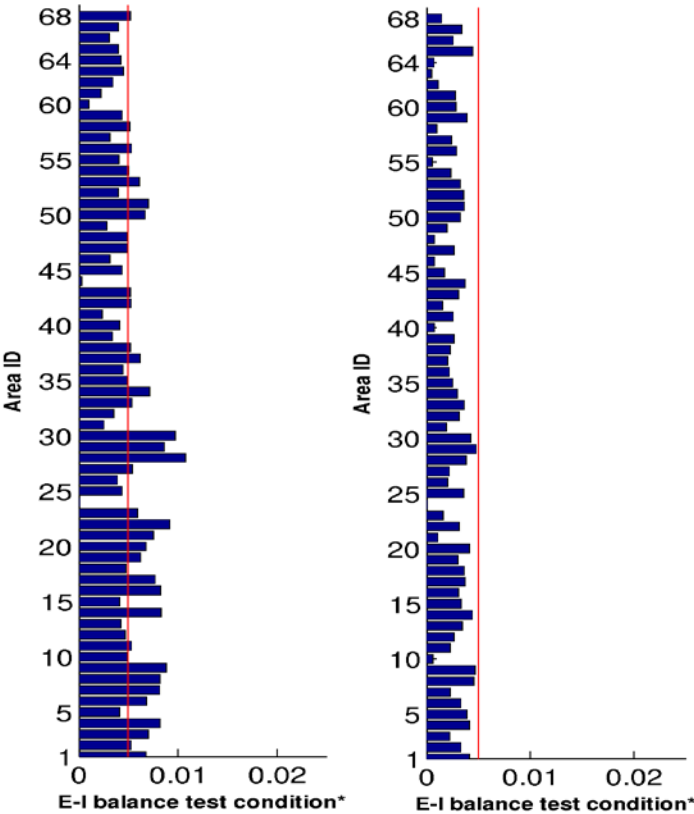
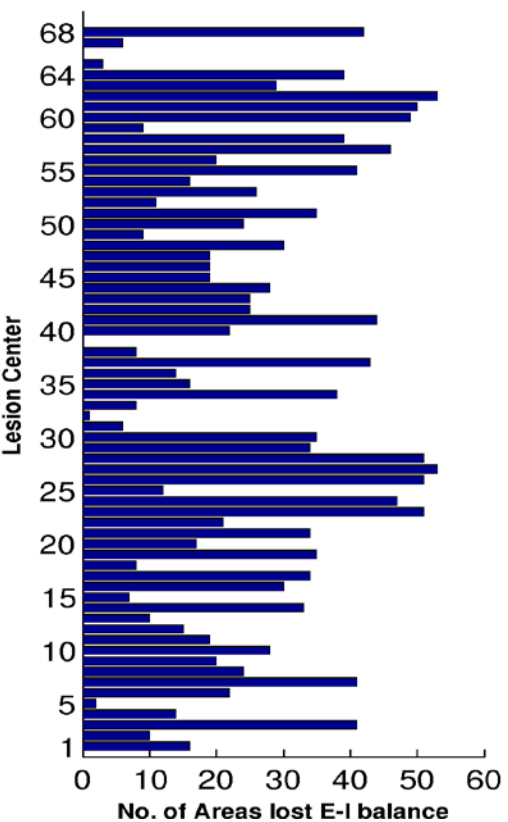


Figure 4:

A



B



C

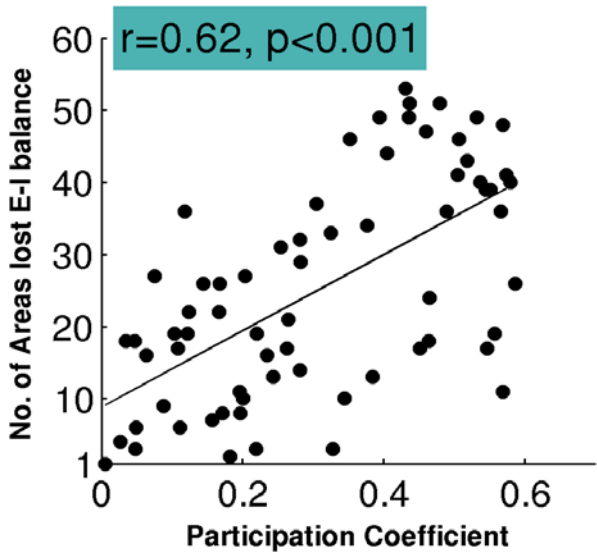
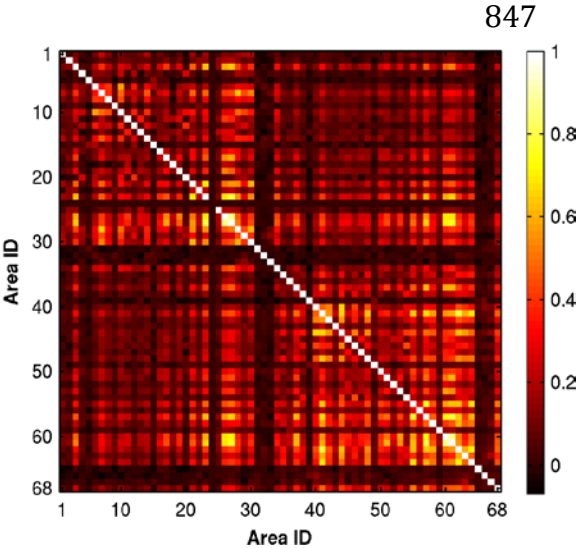


**Figure 5:**

**A**



**B**

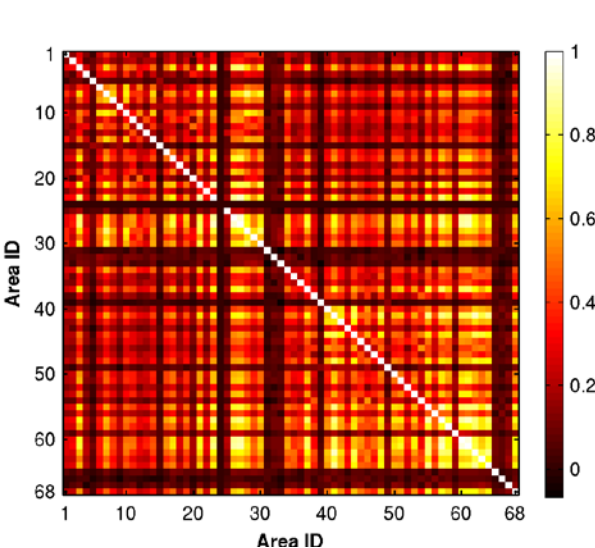
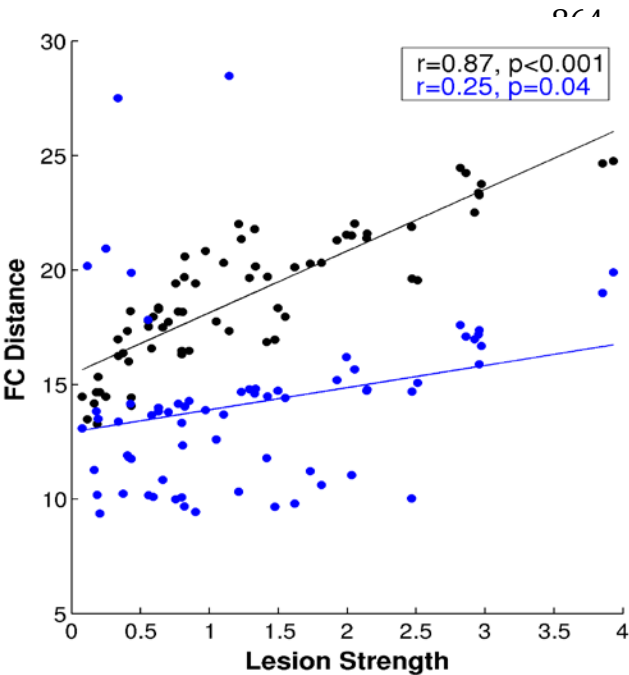


**Figure 6:**

**A**



**B**

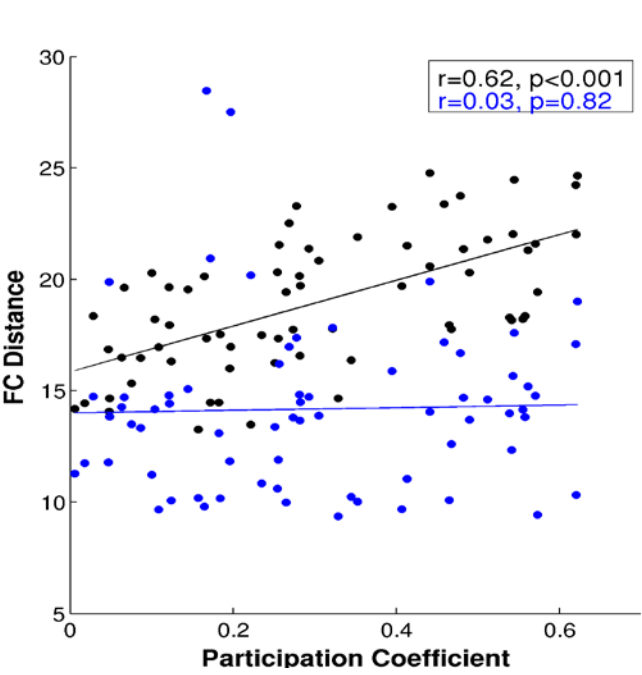
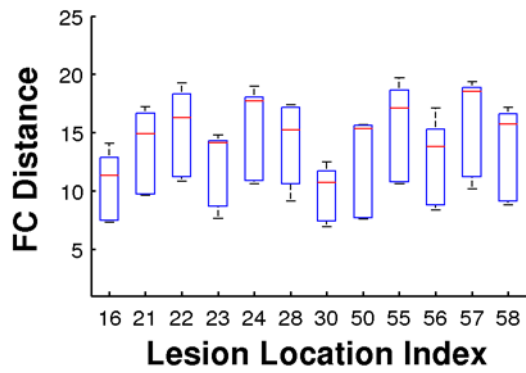


**Figure 7:**

**Figure 8:**

**A**



**B**

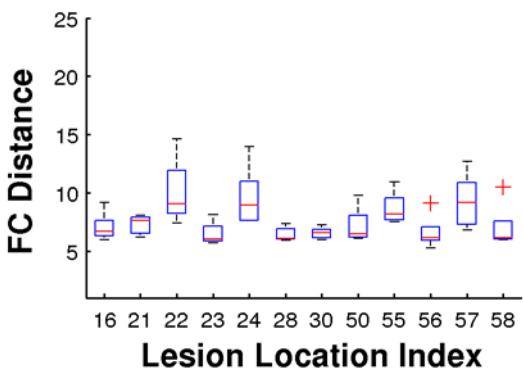


**Table 1:**

Area ID	Abbreviation	Full Name
1	BSTS	Banks Of Superior Temporal Sulcus
2	CAC	Caudal Anterior Cingulate
3	CMF	Caudal Middle Frontal
4	CUN	Cuneus
5	ENT	Entorhinal
6	FUS	Fusiform
7	IP	Inferior Parietal
8	IT	Inferior Temporal
9	ISTH	Isthmus Cingulate
10	LOCC	Lateral Occipital
11	LOF	Lateral Orbito Frontal
12	LING	Lingual
13	MOF	Medial Orbito Frontal
14	MT	Middle Temporal
15	PARH	Parahippocampal
16	PARC	Paracentral
17	POPE	Pars Opercularis
18	PORB	Pars Orbitalis
19	PTRI	Pars Triangularis
20	PCAL	Pericalcarine
21	PCNT	Post Central
22	PC	Posterior Cingulate
23	PREC	Precentral
24	PCUN	Precuneus
25	RAC	Rostral Anterior Cingulate
26	RMF	Rostral Middle Frontal
27	SF	Superior Frontal
28	SP	Superior Parietal
29	ST	Superior Temporal
30	SMAR	Supra Marginal
31	FP	Frontal Pole
32	TP	Temporal Pole
33	TT	Transverse Temporal
34	INS	Insula

**Table 2:**

DMF Model Parameters
<b>Excitatory:</b> $W_E = 1, w_+ = 1.4, J_{NMDA} = 0.15 \text{ nA}$ $a_E = 310 \text{ nC}^{-1}, b_E = 125 \text{ Hz}, d_E = 0.16 \text{ s}$
<b>Inhibitory:</b> $W_I = 0.7, a_I = 615 \text{ nC}^{-1}, b_I = 177 \text{ Hz}$ $d_I = 0.087 \text{ s}$
<b>Kinetic:</b> $\gamma = 0.641 \text{ s}, \tau_E = 100 \text{ ms}, \tau_I = 10 \text{ ms}$

**Table 3:**

	Area	Participation Coefficient	FCD before re-establishing E-I balance	FCD after re-establishing E-I balance
<i>Left Hemisphere</i>				
Cortical midline	PCUN	0.57	21	15
	CAC	0.34	16	10
Parietal and Temporal cortex	<b>IP</b>	<b>0.35</b>	<b>22</b>	<b>10</b>
	SMAR	0.55	22	16
	ST	0.25	20	11
	IT	0.28	20	15
Frontal cortex	SF	0.43	25	20
	<b>CMF</b>	<b>0.51</b>	<b>22</b>	<b>15</b>
	POPE	0.3	21	14
Sensory, Motor	LOCC	0.14	20	15
	PREC	0.53	24	18
<i>Right Hemisphere</i>				
Cortical midline	PCUN	0.51	22	11
	<b>CAC</b>	<b>0.54</b>	<b>18</b>	<b>14</b>
Parietal and Temporal cortex	IP	0.43	23	17
	SMAR	0.55	22	16
	ST	0.23	20	11
	IT	0.25	20	15
Frontal cortex	SF	0.47	25	19
	CMF	0.51	22	10
	POPE	0.29	21	14
Sensory, Motor	LOCC	0.16	20	15
	PREC	0.56	24	17